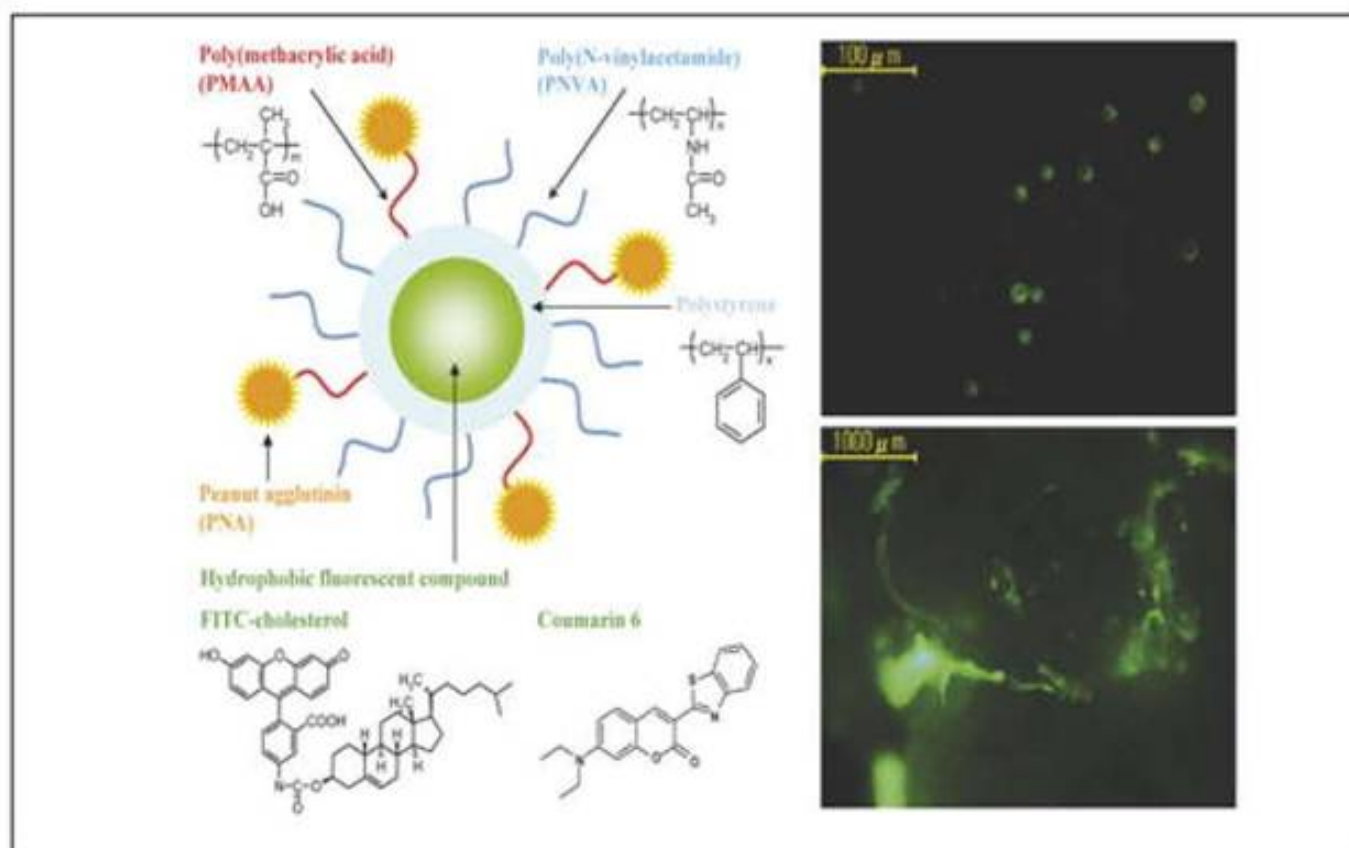




# journal of controlled release

OFFICIAL JOURNAL OF THE CONTROLLED RELEASE SOCIETY  
AND THE JAPANESE SOCIETY OF DRUG DELIVERY SYSTEM



## COVER STORY

In vitro/in vivo biorecognition of lectin-immobilized fluorescent nanospheres for human colorectal cancer cells



Contents lists available at ScienceDirect

Journal of Controlled Release

journal homepage: [www.elsevier.com/locate/jconrel](http://www.elsevier.com/locate/jconrel)

## In vitro/in vivo biorecognition of lectin-immobilized fluorescent nanospheres for human colorectal cancer cells

Shinji Sakuma<sup>a,\*</sup>, Takanori Yano<sup>a</sup>, Yoshie Masaoka<sup>a</sup>, Makoto Kataoka<sup>a</sup>, Ken-ichiro Hiwatari<sup>b</sup>, Hiroyuki Tachikawa<sup>b</sup>, Yoshikazu Shoji<sup>b</sup>, Ryoji Kimura<sup>b</sup>, Huaiyu Ma<sup>c</sup>, Zhijian Yang<sup>c</sup>, Li Tang<sup>c</sup>, Robert M. Hoffman<sup>c,d</sup>, Shinji Yamashita<sup>a</sup>

<sup>a</sup> Faculty of Pharmaceutical Sciences, Setsunan University, 45-1 Nagaotoge-cho, Hirakata, Osaka 573-0101, Japan

<sup>b</sup> Advanced Materials R & D Laboratory, ADEKA Co., 7-2-34 Higashiogu, Arakawa-ku, Tokyo 116-8553, Japan

<sup>c</sup> AntiCancer Inc., 7917 Ostrow Street, San Diego, CA 92111, USA

<sup>d</sup> Department of Surgery, University of California at San Diego, La Jolla, CA 92103-8220, USA

### ARTICLE INFO

#### Article history:

Received 2 September 2008

Accepted 18 October 2008

Available online 31 October 2008

#### Keywords:

Endoscopic imaging agent

Colonoscopy

Colorectal cancer

Orthotopic cancer model

Lectin

### ABSTRACT

Peanut agglutinin (PNA)-immobilized polystyrene nanospheres with surface poly(*N*-vinylacetamide) (PNVA) chains encapsulating coumarin 6 were designed as a novel colonoscopic imaging agent. PNA was a targeting moiety that binds to  $\beta$ -D-galactosyl-(1-3)-*N*-acetyl-D-galactosamine, which is the terminal sugar of the Thomsen–Friedenreich antigen that is specifically expressed on the mucosal side of colorectal cancer cells. PNVA was immobilized with the aim of reducing nonspecific interactions between imaging agents and normal tissues. Coumarin 6 was encapsulated into nanosphere cores to provide endoscopically detectable fluorescence intensity. After incubation of imaging agents with human cells, the fluorescence intensity of imaging agent-bound cells was estimated quantitatively. The average fluorescence intensity of any type of colorectal cancer cell used in this study was higher than that of small intestinal epithelial cells that had not exposed the carbohydrate. The in vivo performance of imaging agents was subsequently evaluated using a human colorectal cancer orthotopic animal model. Imaging agent-derived strong fluorescence was observed at several sites of the large intestinal mucosa in the tumor-implanted nude mice after the luminal side of the colonic loop was contacted with imaging agents. In contrast, when mice that did not undergo tumor implantation were used, the fluorescence intensity on the mucosal surface was extremely low. Data indicated that imaging agents bound to colorectal cancer cells and the cancer cell-derived tumors with high affinity and specificity.

© 2008 Elsevier B.V. All rights reserved.

### 1. Introduction

Colorectal cancer is a major cause of mortality and morbidity in developed countries [1,2]. Currently, surgical removal is the primary treatment of choice, and early detection and resection are indispensable for curing colorectal cancer [2–4]. A fecal occult blood test is widely used as the easiest way of screening for colorectal cancer, although it does not always provide a definitive diagnosis [2,5]. Patients with positive findings need to be diagnosed by subsequent endoscopy in order to visually confirm the existence of cancer [2–6]. Colorectal cancer first develops in the mucous membrane of the large intestine, and invasion and metastasis are observed as the cancer progresses. Colonoscopy performed for the above-mentioned purpose is often accompanied by the resection of cancer that remains in the mucous membrane or only minimally invades the submucosal tissues without vessel invasion [7,8]. This minimally invasive operation,

known as endoscopic mucosal resection (EMR), can serve as an alternative to surgical resection in the early stage of cancer [7–9].

Colonoscopy is the preferred screening method for colorectal cancer because it provides a definitive diagnosis in such cases. EMR prolongs patient survival and enriches quality of life [7–10]. However, a limitation of standard white-light colonoscopy is that it can only detect tumor tissues that are ca.  $\geq 1$  cm in size with a relatively high possibility of metastasis, although the detectable size depends on the cancer type and the skill of the physician [4,10]. Magnifying endoscopy contributes to the early detection of small-sized colorectal cancer; however, real-time and accurate differentiation of neoplastic mucosal changes remains a significant challenge [11,12]. Advances in bioengineering have provided promising revolutionary imaging strategies for endoscopic diagnosis [11–15]. Narrow band imaging (NBI) is a novel technique that enhances the visualization of surface mucosal and vascular patterns. Some studies suggest the clinical usefulness of NBI with magnification for the evaluation of the microvascular architecture and the quantitative diagnosis of colorectal cancer [11,15]. Autofluorescence imaging (AFI) is another new technique that involves the use

\* Corresponding author. Tel.: +81 72 866 3124; fax: +81 72 866 3126.  
E-mail address: [sakuma@pharm.setsunan.ac.jp](mailto:sakuma@pharm.setsunan.ac.jp) (S. Sakuma).

of blue endoscopic light to induce mucosal autofluorescence [14]. Among all spectroscopic techniques, AFI has been the most widely studied for the diagnosis of colorectal cancer, and it has also been used to identify adenomas and dysplasia in inflammatory bowel disease [13].

Imaging agents may also support real-time and accurate diagnosis of early colorectal cancer. Using colorectal cancer-specific cyclic peptides with near-infrared fluorescence imaging probes, Kelly et al. have investigated an imaging agent for endoscopic tumor detection in a murine model [16]. The peptides were administered intravenously to nude mice bearing descending colon tumors derived from the HT-29, human colorectal adenocarcinoma cell line. The internalization of the agent from the bloodstream into the cancer cells that had been implanted orthotopically was observed using a near-infrared fluorescence endoscope.

We have also been investigating a novel endoscopic imaging agent for the early detection of small-sized colorectal cancer [17]. In contrast to the approach of Kelly, we designed a colonoscopic imaging agent that can recognize tumor-derived changes on the mucosal side of the cells in the large intestine with high affinity and specificity. As illustrated in Fig. 1, the agent is composed of submicron-sized fluorescent polystyrene nanospheres with two functional groups – peanut (*Arachis hypogaea*) agglutinin (PNA) and poly(*N*-vinylacetamide) (PNVA) – on their surfaces. The agent targets the Thomsen–Friedenreich (TF) antigen which is specifically expressed on the mucosal side of colorectal cancer cells [18–20]. Its terminal sugar is  $\beta$ -D-galactosyl-(1-3)-*N*-acetyl-D-galactosamine (Gal- $\beta$ (1-3)GalNAc), and this sugar is masked by oligosaccharide side chain extension or sialylation in normal cells [18–21]. Lectins are proteins that recognize and bind reversibly to specific carbohydrate residues expressed on the cell surface [22–25]. PNA is immobilized on the nanosphere surface by the coupling of the amino groups of PNA with the carboxyl groups of poly(methacrylic acid) (PMAA), as a targeting moiety that binds to the TF antigen specifically through the recognition of Gal- $\beta$ (1-3)GalNAc [26–29]. PNVA is a nonionic polymer with strong hydrophilicity. Our past researches have indicated that hydrophilicity-induced thick water layers prevented the materials that were surface-coated with PNVA from interacting with the mucous membrane of the gastrointestinal tract [30–32]. PNVA is immobilized on the nanosphere surface; this enhances the specificity of PNA by reducing the nonspecific interaction between the imaging agents and normal

tissues. In our previous research, a conventional hemagglutination test was performed to evaluate the effect of the chemical structure of the nanosphere surface on the affinity and specificity of the immobilized PNA for the recognition of Gal- $\beta$ (1-3)GalNAc [17]. We consequently obtained PNA-immobilized fluorescent nanospheres with surface PNVA chains whose affinity and specificity for Gal- $\beta$ (1-3)GalNAc detection were equivalent and superior, respectively, to those of intact PNA.

It is anticipated that intracolonic (enema) administration of imaging agents leads to their specific accumulation on the surface of tumor tissues in the large intestine. Real-time and accurate diagnosis of small-sized early colorectal cancer can be subsequently realized through the observation of a clear fluorescence contrast between the normal and tumor tissues under the standard white-light fluorescent endoscope with or without magnification. Intracolonic administered sub-micron sized nanospheres are not absorbed logically through the intestinal membranes. The non-absorption may result in high safety and a low incidence of drug–drug interactions when compared with conventional imaging agents that are administered systemically. Our previous research showed that a hydrophobic fluorescein-labeled compound could be encapsulated efficiently into the hydrophobic polystyrene cores of the nanospheres through strong physicochemical interactions [17]. An endoscopically detectable fluorescence intensity will be achieved by encapsulating a sufficient amount of the fluorescein-labeled compound. Here, we report the quantitative evaluation of the fluorescence intensity and our novel findings on the *in vitro/in vivo* biorecognition of imaging agents against various human colorectal cancer cells/orthotopic human colorectal tumors in nude mice.

## 2. Materials and methods

### 2.1. Materials

NVA monomers were gifted by Showa Denko Co. (Tokyo, Japan). Coumarin 6, a fluorescein-labeled compound used in this study, and PNA were obtained from Sigma–Aldrich (St. Louis, MO, USA). Fluorescein isothiocyanate (FITC)-PNA was purchased from J-Oil Mills Inc. (Tokyo, Japan). All other chemicals were commercial products of reagent grade. Styrene was purified by distillation under reduced pressure, and 2, 2'-azobisisobutyronitrile (AIBN) was purified by recrystallization from acetone. All other chemicals were used without further purification.

Human colorectal adenocarcinoma cell lines, HT-29, HCT-116, LS174T, HCT-15, and SW480, were purchased from Dainippon–Sumitomo Pharma Biomedical Co. Ltd. (Osaka, Japan), and Caco-2 was obtained from the American Type Culture Collection (Rockville, MD, USA). A human breast ductal carcinoma cell line, T47D, and cultured human small intestinal epithelial cells were obtained from Dainippon–Sumitomo Pharma Biomedical Co. Ltd. The following media were obtained from Sigma–Aldrich: RPMI-1640 Medium; McCoy's 5A Medium, Modified (with sodium bicarbonate, without L-glutamine); Minimum Essential Medium Eagle; Dulbecco's Modified Eagle's Medium; L-15 Medium; Dulbecco's Phosphate Buffered Saline (PBS with calcium chloride and magnesium chloride); Dulbecco's Phosphate Buffered Saline, Modified (PBS without the divalent metal ions). CSF-4KO-500D, which is a medium kit for cultured small intestinal epithelial cells, was provided by the manufacturer of the cells. Fetal bovine serum (FBS), heat-inactivated FBS, penicillin (10,000 U/mL), streptomycin (10 mg/mL), L-glutamine (200 mM), non-essential amino acids (10 mM), and trypsin-EDTA (0.25% trypsin and 1 mM EDTA) were purchased from GIBCO Laboratories (Lenexa, KS, USA). Blocker Casein in PBS was obtained from Thermo Fisher Scientific Inc. (Rockford, IL, USA). Anti-TF pan-tumor antigen (A78-G/A7) was purchased from American Research Products Inc. (Belmont, MA, USA). Mouse IgM was obtained from DAKO (Glostrup, Denmark). Alexa Fluor 488-labeled goat anti-mouse IgM antibody was purchased from Invitrogen Inc. (Carlsbad, CA, USA). Preserved rabbit blood and neuraminidase (sialidase, 1 unit/mL,

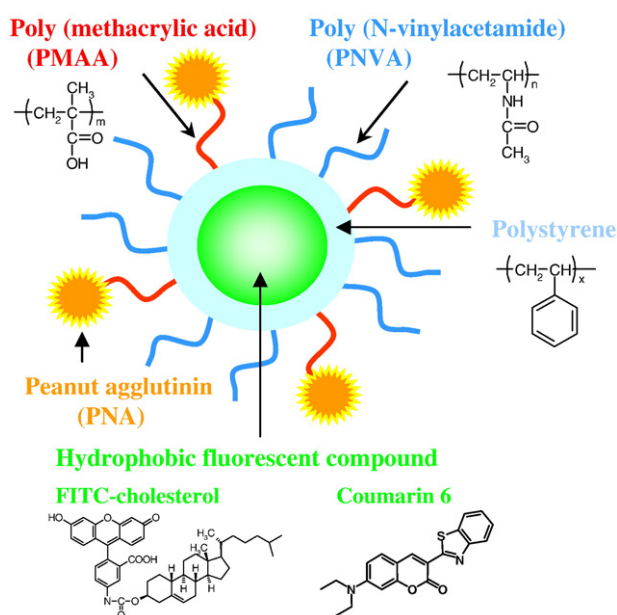


**Fig. 1.** Schematic representation of PNA-immobilized fluorescent nanospheres with surface PNVA chains encapsulating hydrophobic fluorescent compounds.

extracted from *Arthrobacter ureafaciens*) were obtained from Nippon Bio-Test Laboratories Inc. (Tokyo, Japan) and Roche Diagnostics (Indianapolis, IN, USA), respectively.

The pLNC<sub>x2</sub> vector, which contains the neomycin resistance gene for antibiotic selection in eukaryotic cells, the red fluorescent protein (RFP, DsRed2), and RePT67 (an NIH 3T3-derived packaging cell line expressing the 10 A1 viral envelope) were purchased from Clontech (Mountain View, CA, USA). G418, a precipitated mixture of *N*-[1-(2,3-dioleoyloxy)propyl]-*N,N,N*-trimethylammonium methylsulfate reagent, and cloning cylinders were obtained from Roche Molecular Biochemicals (Indianapolis, IN, USA), Life Technologies (Grand Island, NY, USA), and Bel-Art Products (Pequannock, NJ, USA), respectively.

## 2.2. Preparation of PNA-immobilized fluorescent nanospheres with surface PNVA chains (imaging agents)

Imaging agents were prepared in the same manner as that described in our previous article [17], with the exception that coumarin 6 was encapsulated into nanosphere cores in the process of dispersion copolymerization between vinylbenzyl group-terminated PNVA, vinylbenzyl group-terminated PMAA, and styrene.

PNVA and poly(*tert*-butyl methacrylate) (PBMA) were prepared by the free radical polymerization of NVA and butyl methacrylate (BMA) monomers, respectively, in the presence of 2-mercaptoethanol. The resulting hydroxyl group-terminated PNVA and PBMA were reacted with *p*-chloromethyl styrene in the presence of tetrabutylphosphonium bromide in an alkaline solution. Vinylbenzyl group-terminated PMAA was obtained by hydrolyzing vinylbenzyl group-terminated PBMA in an acidic solution with hydroquinone.

Vinylbenzyl group-terminated PNVA (0.5 g), vinylbenzyl group-terminated PMAA (0.5 g), and styrene (1.0 g) were dissolved in 15 mL of ethanol/water mixture (2/1, v/v) containing AIBN (ca. 1 mol% of the total monomers) and coumarin 6 (0.1% of the total monomers). The solution was bubbled with nitrogen for 30 min, and the tube was then sealed. Dispersion copolymerization was successively carried out at 60 °C for 18 h under mild stirring. After the centrifugation of the resulting nanosphere dispersion (6200 g, 15 min), the supernatant containing the unreacted substances and unencapsulated coumarin 6 was removed, and the precipitated nanospheres were dispersed into the ethanol/water mixture. This process was repeated 3 times. The precipitated fluorescent nanospheres with surface PNVA and PMAA chains (platforms of imaging agents) were finally dispersed in purified water and lyophilized.

In order to estimate the encapsulation properties of coumarin 6, fluorescent nanospheres with only surface PNVA chains were prepared at a different concentration of the dye during the copolymerization. Vinylbenzyl group-terminated PNVA (1.0 g) and styrene (1.0 g) were dissolved in 15 mL of the ethanol/water mixture containing AIBN (ca. 1 mol% of the total monomers) and coumarin 6 (0.1–1% of the total monomers). The nanospheres were prepared in the same manner as that described in the previous paragraph.

PNA was bound to the fluorescent nanospheres with surface PNVA and PMAA chains encapsulating coumarin 6 through the coupling of amino groups of PNA with carboxyl groups of PMAA activated by pre-incubation with 1-ethyl-3-(3-dimethylaminopropyl) carbodiimide. The resulting PNA-immobilized fluorescent nanospheres with surface PNVA chains (imaging agents) were purified by changing the dispersion media several times, and finally dispersed in purified water at a concentration of 20 mg/mL.

## 2.3. Characterization

### 2.3.1. Routine characterization

Routine characterization of the imaging agent and its platform were performed as described in our previous articles [17,30–36]. Briefly, weight- and number-average molecular weights (*M<sub>w</sub>*/*M<sub>n</sub>*) of

the surface PNVA and PMAA chains were determined by gel permeation chromatography. The nanosphere size was measured by dynamic light-scattering spectrophotometry. The zeta potential of the nanospheres was measured by electrophoretic light-scattering spectrophotometry in PBS (without divalent metal ions). The ratio of the number of NVA units to that of MAA units on the nanosphere surface was evaluated by electron spectroscopy for chemical analysis (ESCA). The amount of PNA immobilized on the nanosphere surface was measured by the ninhydrin method. The affinity and specificity of PNA immobilized on the nanosphere surface for the recognition of Gal-β(1–3)GalNAc was evaluated using the hemagglutination test.

### 2.3.2. Assay of coumarin 6 encapsulated into the nanosphere cores

Fluorescent nanospheres with only surface PNVA chains were dissolved in chloroform at a concentration of 2.5 mg/mL. Coumarin 6 dissolved in the solution was assayed by measuring the absorption at 445 nm using a UV-Vis spectrophotometer (V-550, JASCO Co., Tokyo, Japan). When necessary, the solution was diluted with chloroform. The calibration curve of coumarin 6 was prepared in the range of 0.1 µg/mL to 5 µg/mL.

### 2.3.3. Leakage of coumarin 6 from the fluorescent nanospheres

Fluorescent nanospheres with only surface PNVA chains were dispersed in PBS (with divalent metal ions) at a concentration of 10 mg/mL. The dispersion was incubated at 37 °C for 3 h. After centrifugation of the dispersion (18,400 g, 15 min), coumarin 6 in the supernatant was assayed by UV-Vis spectrophotometry, as described above.

### 2.3.4. Quantitative evaluation of fluorescence intensity of the fluorescent nanospheres

The fluorescent nanospheres were dispersed in PBS (with divalent metal ions) at a concentration of 1 mg/mL. The fluorescent microphotograph was measured using a fluorescence microscope at an excitation of 470–495 nm, an emission of 510–550 nm, and an exposure of 1/60 of a second (IX71-22FL/PH, Olympus Co., Ltd., Tokyo, Japan). The fluorescence intensity of the nanosphere was quantitatively estimated using an image analysis tool (LuminaVision, Mitani Co., Ltd., Tokyo, Japan). In the analysis program, the lower limit of the fluorescence in the microphotographs that were used for the estimation was set as 14.

## 2.4. In vitro biorecognition of imaging agents against various human cells

### 2.4.1. Cell culture

Cells were seeded at a density of  $2 \times 10^4$  cells/mL (HT-29 and HCT-116),  $6 \times 10^4$  cells/mL (T47D, LS174T, HCT-15, Caco-2, and SW480), or  $10 \times 10^4$  cells/mL (small intestinal epithelial cells) in a flask of adequate volume (25–75 mL). The cells were grown as a monolayer in the media summarized in Table 1 and were maintained at 37 °C in a humidified atmosphere of 95% O<sub>2</sub>/5% CO<sub>2</sub>; SW480 was an exception (these cells were maintained in a humidified atmosphere of 100% air). Cells were then routinely passaged when they became 100% confluent, and the narrow passage cell lines (passage: ≤10 times) were used for all studies.

### 2.4.2. Immunofluorometric cell staining

A cover glass was placed at the bottom of the flask. The cells were seeded, grown, and maintained in the same manner as that described in the previous section. When confluent, the cover glass was picked out along with the cell monolayer. The cover glass was washed with PBS (without divalent metal ions) and was then immersed in ethanol containing acetic acid (1%, v/v) at 4 °C for 10 min. Cells immobilized on the cover glass were washed 5 times with PBS and were kept for 30 min in Blocker Casein in PBS at room temperature. The cells were

**Table 1**  
Culture media for respective cells

| Cell lines                    | Media   |
|-------------------------------|---|
| T47D                          | RPMI-1640 Medium supplemented with 100% (v/v) FBS, 50 U/ml penicillin, and 50 µg/ml streptomycin  |
| HT-29                         | McCoy's 5A Medium, Modified supplemented with 10% (v/v) FBS, 50 U/ml penicillin, 50 µg/ml streptomycin, and 1.5 mM L-glutamine                      |
| HCT-116                       | McCoy's 5A Medium, Modified supplement with 10% (v/v) FBS, 50 U/ml penicillin, 50 µg/ml streptomycin, and 1.5 mM L-glutamine                        |
| LS174 T                       | Minimum Essential Medium Eagle supplemented with 10% (v/v) FBS, 50 U/ml penicillin, 50 µg/ml streptomycin, and 0.1 mM non-essential amino acids     |
| HCT-15                        | RPMI-1640 Medium supplemented with 20% (v/v) heat-inactivated FBS, 50 U/ml penicillin, and 50 µg/ml streptomycin                                    |
| Caco-2                        | Dulbecco's Modified Eagle's Medium supplemented with 10% (v/v) FBS, 50 U/ml penicillin, 50 µg/ml streptomycin, and 0.1 mM non-essential amino acids |
| SW480                         | L-15 Medium supplemented with 10% (v/v) FBS, 50 U/ml penicillin, 50 µg/ml streptomycin, and 1.5 mM L-glutamine                                      |
| Epithelial cells <sup>a</sup> | CSF-4KO-500D <sup>b</sup>   |

<sup>a</sup> Epithelial cells of the small intestine in humans.

<sup>b</sup> A medium kit supplied from Dainippon-Sumitomo Pharma Biomedical Co. Ltd. (Osaka, Japan).

subsequently reacted for 1 h with anti-TF pan-tumor antigens (diluted 10 times with Blocker Casein in PBS, 100 µL) at room temperature. As a negative control, mouse IgM was used (diluted 100 times with Blocker Casein in PBS, 10 µg/mL, 100 µL). The cells were washed 5 times with PBS and then reacted with labeled goat anti-mouse IgM antibodies (diluted 200 times with Blocker Casein in PBS, 10 µg/mL, 100 µL) at room temperature for 1 h. After washing the cells 5 times with PBS, the excess water in the cover glass was removed. Glycerol was dropped into the cover glass, and the cover glass was then inverted over the slide glass. The fluorescence microphotograph was measured using a fluorescence microscope at an excitation of 495 nm and an emission of 519 nm with auto exposure (BX60, Olympus Co., Ltd.).

#### 2.4.3. *In vitro* biorecognition of imaging agents against various human cells

Cells were washed with 20 mL of PBS (without divalent metal ions) after the removal of the culture media. PBS was removed, and the cells were treated at 37 °C for 3 min with 2 mL of the aqueous solution containing trypsin-EDTA. A corresponding culture medium (10 mL) was added to remove the cells from the flask. The collected cells were centrifuged at 180 g for 10 min, and the precipitated cells were suspended in PBS (with divalent metal ions) at a concentration of  $1 \times 10^7$  cells/mL. Separately, the imaging agents were dispersed in PBS (with divalent metal ions) at a concentration of 4 mg/mL, and the dispersion was then mixed with an equivalent volume of cell suspension. The mixture was incubated at 37 °C for 30 min and then centrifuged at 180 g for 5 min to separate the cells from the unbound imaging agents. The imaging agent-bound cells were re-suspended in the PBS, and fluorescence microphotographs were obtained using the fluorescence microscope (excitation: 470–495 nm; emission: 510–550 nm; exposure: 1/60 of a second). The fluorescence intensity of the cells was quantitatively estimated using the image analysis tool. The biorecognition experiment was also carried out by substituting the imaging agent with FITC-PNA. The PNA concentration of FITC-PNA was adjusted to be equivalent to that of the imaging agent. The fluorescence intensity of the FITC-PNA-bound cells was evaluated in the same manner as that described above.

#### 2.5. *In vivo* biorecognition of imaging agents against orthotopic human colorectal tumors

##### 2.5.1. Preparation of nude mice bearing ascending colon tumors

A red fluorescent protein (RFP)-expressing orthotopic human colorectal cancer model was constructed as follows [37–40]. All

animal studies were conducted in accordance with the principles and procedures outlined in the National Institute of Health Guide for the Care and Use of Animals under Assurance Number A3873-1.

The RFP was inserted in the pLNC<sub>x2</sub> vector at the *EgIII* and *NotI* sites. PT67 cells were cultured in Dulbecco's Modified Eagle's Medium supplemented with 10% (v/v) heat-inactivated FBS. For vector production, packaging cells (PT67), at 70% confluence, were incubated with a precipitated mixture of *N*-[1-(2,3-dioleoyloxy)propyl]-*N,N,N*-trimethylammonium methylsulfate reagent and saturating amounts of pLNC<sub>x2</sub>-DsRed2 plasmid for 18 h. Fresh medium was replenished at this time. The cells were examined by fluorescence microscopy 48 h after transfection. For selection, the cells were cultured in the presence of 500–2000 µg/mL of G418 for 7 days.

For RFP gene transduction, 25% confluent HT-29 cells were incubated with a 1:1 precipitated mixture of retroviral supernatants of PT67 cells and RPMI 1640 Medium containing 10% (v/v) FBS for 72 h. Fresh medium was replenished at this time. Cells were harvested by trypsin-EDTA 72 h after transduction, and subcultured at a ratio of 1:15 into a selective medium that contained 200 µg/mL of G418. The level of G418 was increased to 400 µg/mL in a stepwise manner. Clones stably expressing RFP were isolated with cloning cylinders by trypsin-EDTA and were then amplified, and transferred by conventional culture methods in the absence of a selective agent.

Nude mice, 4-week-old outbred nu/nu female mice, were used for tumor implantation. A tumor stock of HT-29-RFP was established by subcutaneously injecting HT-29-RFP cells ( $1 \times 10^6$  cells/mL) into the flank of nude mice at a dose of 0.05 mL/mouse. The tumor was maintained in the nude mice subcutaneously as tumor stock prior to being used. On the day of implantation, the tumor was harvested from the subcutaneous site and placed in RPMI-1640 Medium. Strong RFP expression of the HT-29-RFP tumor tissues was confirmed by fluorescence imaging. Necrotic tissues were removed and viable tissues were cut into 1 mm<sup>3</sup> pieces. The nude mice were transplanted by surgical orthotopic implantation using tumor tissue fragments harvested from the stock tumors. The animals were anesthetized with a mixture of ketamine, acepromazine, and xylazine, and the surgical area was sterilized using iodine solution and alcohol. An incision approximately 1.5 cm long was made along the left lateral abdomen of the nude mouse using a pair of sterile scissors. After the abdomen was opened, the ascending colon was exposed. The serosa of the transplantation site had been stripped. Two fragments of 1 mm<sup>3</sup> of the HT-29-RFP tumor tissue were sutured adjacent to each other onto the ascending colon with a sterile 8–0 surgical suture (nylon) to generate only one primary tumor. The abdomen was closed using sterile 6–0 surgical sutures (silk). All surgical procedures and animal manipulations were conducted under HEPA-filtered laminar-flow hoods.

##### 2.5.2. *In vivo* biorecognition of imaging agents against orthotopic human colorectal tumors

Animal experiments were approved by the Ethical Review Committee of Setsunan University. Nude mice bearing ascending colon tumors were fasted for 24 h with free access to water before experiments. Under ether anesthesia, the abdomen was opened and the ascending colon in which HT-29-RFP tumor tissues were implanted was observed. An approximately 3-cm loop of the ascending colon bearing tumor tissues was prepared in the abdomen by ligating both ends of the colon after washing its luminal side with saline. The imaging agents were dispersed in PBS (with divalent metal ions) at a concentration of 4 mg/mL, and 1.0 ml of the dispersion was injected into the loop. At 30 min after injection, the loop was removed and its luminal side was washed with 1.0 mL of PBS (with divalent metal ions). The colon was cut longitudinally and the fluorescence microphotograph of the mucosal surface was measured using the fluorescence microscope (excitation: 470–495 nm; emission: 510–550 nm; exposure: 1/15 to 1/60 of a second). As a control, normal nude mice that did not undergo tumor implantation were tested in the same manner as that described above. For the evaluation of the

autofluorescence of normal and tumor tissues in the colon, an equivalent volume of PBS (with divalent metal ions) was substituted for the dispersion of the imaging agents.

### 3. Results and discussion

#### 3.1. Quantitative evaluation of the fluorescence intensity of fluorescent nanospheres with only surface PNVA chains encapsulating coumarin 6

Polymeric nanospheres composed of graft copolymers having a hydrophobic polystyrene backbone and hydrophilic polyvinyl branches were used as platforms for the imaging agents. The nanospheres, which have been thoroughly investigated by Akashi and his co-workers [30–36], are spherical particles whose size is adjusted to the magnitude of  $10^2$  nm and whose hydrophobic polystyrene core is covered with hydrophilic polyvinyl chains (core-corona type structure). By changing the chemical structure of the polyvinyl chains, nanospheres with diverse surface properties can be obtained. Furthermore, macromolecules such as lectins can be immobilized chemically on the surface of nanospheres via linkers such as PMAA. Hydrophobic compounds with small molecular weights can be incorporated into the hydrophobic core through physicochemical interactions.

In our previous research, we newly synthesized fluorescein-labeled cholesterol as the hydrophobic fluorescein-labeled compound [17]. The fluorescein-labeled cholesterol was encapsulated efficiently and strongly into the hydrophobic polystyrene core of the nanospheres. Individual PNA-immobilized nanospheres with surface PNVA chains encapsulating the fluorescein-labeled cholesterol were observed under fluorescence microscopy, although the purity of the cholesterol was 6% (94% was unreacted cholesterol without a fluorescent probe). The mass balance study also indicated that fluorescein-labeled cholesterol is a potent candidate for a hydrophobic fluorescein-labeled compound that provides endoscopically detectable fluorescence intensity. However, a modification process yielding highly pure fluorescein-labeled cholesterol could not be established.

Therefore, fluorescein-labeled cholesterol was replaced with coumarin 6, a commercial hydrophobic product having a high fluorescent quantum efficiency and a fluorescence spectrum similar to that of fluorescein-labeled cholesterol. Table 2 shows the encapsulation properties of coumarin 6 into fluorescent nanospheres with only surface PNVA. Vinylbenzyl group-terminated PNVA was copolymerized with styrene in the ethanol/water mixture (2/1, v/v) containing coumarin 6 in the absence of vinylbenzyl group-terminated PMAA because PMAA is insoluble in chloroform that was used as a solvent to extract coumarin 6 from the nanospheres. The weight of coumarin 6 encapsulated into the fluorescent nanospheres per gram of the nanospheres roughly corresponded to the ratio of the concentration of the dye to that of the total monomers in the 0.1% to 0.5% region (Runs 1–3). The mass balance of coumarin 6 in that range was  $\geq 20\%$ , which was comparable to the yield of nanospheres. These data indicated that most coumarin 6 would be encapsulated into nanospheres when the yield approached 100%. When the ratio of the concentration of coumarin 6 to that of the total monomers was elevated to 1.0% (Run 4), the weight percentage of the dye in the nanospheres remained about 0.5%, and the mass balance reduced to about 10%, although the yield was constant. The solvent became turbid at the elevated concentration of the dye before copolymerization. Since the water solubility of coumarin 6 is extremely low, it appeared that an increased ratio of ethanol in the solvent would be useful for improving the encapsulation properties of the dye. The strength of the fluorescence intensity obtained from image analysis was consistent with the weight percentage of coumarin 6 in the nanospheres. After incubation of the fluorescent nanospheres at 37 °C for 3 h in PBS, no peak was visible at 445 nm, which, if present, would have been derived from coumarin 6, in the supernatant. The absence of a measurable leakage of coumarin 6 from the fluorescent nanospheres

**Table 2**  
Encapsulation properties of coumarin 6 into fluorescent nanospheres with only surface PNVA chains

| Run | Amount of coumarin 6 <sup>a</sup> | Yield of nanospheres <sup>b</sup> | Coumarin 6 encapsulated <sup>c</sup> | Mass balance <sup>d</sup> | Fluorescence intensity <sup>e</sup> | Leakage <sup>f</sup> |
|-----|-----------------------------------|-----------------------------------|--------------------------------------|---------------------------|-------------------------------------|----------------------|
| 1   | 0.1                               | 29                                | 0.10                                 | 29                        | 26.8 ± 5.74                         | n.d. <sup>g</sup>    |
| 2   | 0.3                               | 20                                | 0.35                                 | 23                        | 39.3 ± 10.3                         | n.d. <sup>g</sup>    |
| 3   | 0.5                               | 33                                | 0.44                                 | 29                        | 59.6 ± 13.6                         | n.d. <sup>g</sup>    |
| 4   | 1.0                               | 26                                | 0.43                                 | 11                        | 63.0 ± 15.2                         | n.d. <sup>g</sup>    |

<sup>a</sup> Coumarin 6 applied in the copolymerization (to total monomers (% w/w)).

<sup>b</sup> Calculated from the weight of lyophilized fluorescent nanospheres with only surface PNVA chains encapsulating coumarin 6 (% w/w).

<sup>c</sup> Calculated from the weight of coumarin 6 encapsulated in the fluorescent nanospheres per gram of the nanospheres (% w/w).

<sup>d</sup> Calculated from the weight ratio of coumarin 6 encapsulated in the fluorescent nanospheres to the dye applied in the copolymerization (% w/w).

<sup>e</sup> Obtained from image analysis of fluorescence microphotographs of the fluorescent nanospheres (mean ± s.d.,  $n > 250$  nanospheres).

<sup>f</sup> Calculated from the amount of coumarin 6 released from the fluorescent nanospheres that were redispersed in PBS with calcium and magnesium ions (% w/w).

<sup>g</sup> Not detected (Lower limit of quantification (0.1 µg/mL) corresponds to 1% of coumarin 6 released from nanospheres when Run 1 is used).

indicated a strong hydrophobic interaction between the dye and the polystyrene core (encapsulation efficiency: 100%).

Akashi et al. found that the core-corona type structure of nanospheres and the polarity of the solvent in the copolymerization between the hydrophilic vinylbenzyl group-terminated polyvinyl compounds and the hydrophobic styrene were closely linked [35]. Since the highly polar ethanol/water mixture is generally utilized as the solvent, the hydrophobic core-hydrophilic corona type structure is formed to stabilize the interface between the solid nanospheres and the liquid solvent. It was probable that the hydrophobic coumarin 6 was efficiently encapsulated into the polystyrene cores during the formation of the core-corona type structure of the nanospheres according to the principles of thermodynamic stability. Consequently, we decided to use coumarin 6 as the hydrophobic fluorescent compound that provides an endoscopically detectable fluorescence intensity.

#### 3.2. Characterization of the fluorescent nanospheres with surface PNVA and PMAA chains and PNA-immobilized ones

The biorecognition of lectins can be evaluated using the hemagglutination test [17]. Since a lectin molecule possesses several sites that bind the carbohydrate residues on the erythrocyte surface, a cross-linking network is formed between the lectins and erythrocytes, thereby inducing erythrocyte agglutination. MAC, i.e., the minimum concentration of lectins that induces erythrocyte agglutination, decreases with an increase in the affinity of lectins for the corresponding carbohydrate residues. Gal-β(1-3)GalNAc, which is recognized by PNA, is expressed on the surface of the erythrocytes that have been pretreated with neuraminidase. The specificity of PNA for this carbohydrate can be estimated by comparing the MACs for neuraminidase-treated and neuraminidase-untreated erythrocytes. The ratio of the MACs (i.e., MAC for neuraminidase-untreated erythrocytes/MAC for neuraminidase-treated erythrocytes) increases with an increase in the specificity. The average MAC of intact PNA was 0.39 µg/mL and 5.7 µg/mL for neuraminidase-treated and neuraminidase-untreated erythrocytes, respectively. Our previous research showed that PNA was immobilized actively on the surface of the nanospheres [17]. The molecular weights of the surface PNVA and PMAA chains affected the affinity and specificity of PNA most strongly, although PNA activity was also influenced by the amount of immobilized PNA and the ratio of the number of NVA units to that of MAA units. When the weight-average molecular weight of PNVA was nearly equal to that of PMAA, the affinity of the PNA immobilized on the nanosphere surface for recognition of Gal-β(1-3)GalNAc was as

**Table 3**  
Characterization of fluorescent nanospheres with surface PNVA and PMAA chains and PNA-immobilized ones

| Characterization  | Fluorescent nanospheres with surface PNVA and PMAA chains | PNA-immobilized fluorescence nanospheres with surface PNVA chains |
|---|---|---|
| Average molecular weight of PNVA (Mw/Mn)                | 9500/4000   | ←   |
| Average molecular weight of PMAA (Mw/Mn)                | 10,000/5600   | ←   |
| Particle size (nm) <sup>a</sup>                         | 243 ± 35  | n.t. <sup>i</sup>   |
| Zeta potential (mV)                                     | -10.9   | n.t. <sup>i</sup>   |
| NVA/MAA <sup>b</sup>                                    | 0.40/0.60   | ←   |
| Coumarin 6 encapsulated (% w/w) <sup>c</sup>            | 0.17 <sup>b</sup>   | n.t. <sup>i</sup>   |
| Fluorescence intensity <sup>d</sup>                     | n.t. <sup>i</sup>   | 33.4 ± 23.0   |
| Immobilized PNA (μg/mg) <sup>e</sup>                    | – <sup>j</sup>  | 5.3   |
| MAC for erythrocytes (μg/mL) <sup>f</sup>               | – <sup>j</sup>  | 125   |
| MAC for neuraminidase-treated ones (μg/mL) <sup>g</sup> | – <sup>j</sup>  | 1.0   |

<sup>a</sup> Weight-average diameter (mean ± s.d.).

<sup>b</sup> Ratio of the number of NVA units to that of MAA units on the nanosphere surface calculated from ESCA spectra.

<sup>c</sup> The weight of coumarin 6 encapsulated in the fluorescent nanospheres per gram of the nanospheres.

<sup>d</sup> Numerical value estimated from image analysis of fluorescence microphotographs of the fluorescent nanospheres (mean ± s.d.,  $n > 250$  nanospheres).

<sup>e</sup> Immobilized amount (μg) of PNA per milligram of nanospheres.

<sup>f</sup> Minimum concentration of PNA immobilized on the nanosphere surface that induced erythrocyte agglutination.

<sup>g</sup> Minimum concentration of PNA immobilized on the nanosphere surface that induced neuraminidase-treated erythrocyte agglutination.

<sup>h</sup> Calculated from the residual amount of coumarin 6 in the solvent after copolymerization and the yield of nanospheres.

<sup>i</sup> Not tested.

<sup>j</sup> Not required.

strong as that of the intact PNA; the specificity for the carbohydrate residue was higher than that of the PNA (the average MAC of immobilized PNA was 1.0 μg/mL and 62.5 μg/mL for neuraminidase-treated and neuraminidase-untreated erythrocytes, respectively). This result indicated that PNVA enhanced the specificity of PNA through the reduction of nonspecific interactions between the PNA and carbohydrates other than Gal-β(1-3)GalNAc on the erythrocyte surface.

The preparation of PNA-immobilized fluorescent nanospheres with surface PNVA chains was repeated using coumarin 6 instead of fluorescein-labeled cholesterol. PNVA with an Mw/Mn of 9500/4000 and PMAA with an Mw/Mn of 10,000/5600 were used. The concentration of coumarin 6 was adjusted to 0.1% of the total monomers. Table 3 summarizes the characterization of the fluorescent nanospheres with the surface PNVA and PMAA chains (platforms of imaging agents) and the PNA-immobilized ones (imaging agents). The yield of the fluorescent nanospheres with surface PNVA and PMAA chains was 29%. Since chloroform-insoluble PMAA was immobilized on the nanosphere surface, the mass balance was calculated from the residual amount of coumarin 6 in the solvent remaining after copolymerization, and 48% of coumarin 6 applied in the copolymerization was observed to have been encapsulated into the nanospheres. The estimated yield and mass balance suggested that the weight of coumarin 6 encapsulated into the fluorescent nanospheres per gram of the nanospheres was 0.17%. The addition of PMAA enhanced the encapsulation of coumarin 6 that was concomitant with the formation of the core-corona type structure. The ionization of the corona layer may result in a clearer phase separation in comparison with the nanospheres with only surface nonionic PNVA chains. The PNA-immobilized fluorescent nanospheres with the surface PNVA chains thus obtained possessed good water dispersibility with no detectable leakage of coumarin 6. The increased fluorescence intensity of the imaging agents reflected an increased amount of coumarin 6

encapsulated into the nanospheres. The other characteristics were similar to those described in our previous article [17].

### 3.3. Specificity of the imaging agent against various types of human colorectal cancer cell lines

Carbohydrates are found on the surfaces of almost all cells in the form of glycoproteins, glycolipids, and polysaccharides [41]. Cell surface glycoproteins are integral components that regulate cell-to-cell interactions and act as receptors for a number of different ligands such as lectins and antibodies [21,42]. Several research groups have been attempting to utilize the biorecognizable interactions between ligands and carbohydrates for site-specific drug delivery [17,22–29].

Ligands with fluorescent probes are often used for the visual evaluation of biorecognition [26–28,43]. When fluorescein-labeled ligands are incubated with cells that have corresponding carbohydrate residues, they bind to the cells specifically as do intact ligands. Therefore, under fluorescence microscopy, biorecognition can be evaluated by measuring the fluorescence of the cells derived from the ligands. Image analysis of the microphotograph also contributes to the quantitative evaluation of the fluorescence intensity of the ligand-bound cells. T47D, a human breast ductal carcinoma cell line, is a typical cell that has the TF antigen [44]. Immunofluorometric cell staining supported the fact that the antigen was obviously expressed on the surface of T47D cells (data not shown). We first examined the biorecognition of the imaging agent (PNA-immobilized fluorescent nanospheres with the surface PNVA chains encapsulating coumarin 6) against cells with exposed Gal-β(1-3)GalNAc by using TF antigen-expressing T47D cells as a positive control. Fig. 2 shows the fluorescence microphotograph of the T47D cells incubated with the imaging agents in PBS. Since PNA is a C-type lectin that requires calcium ions for carbohydrate binding, calcium ion-containing PBS was used as a medium. As shown in Fig. 2, each of the T47D cells was clearly observed with a strong fluorescence. Image analysis estimated that the fluorescence intensity of the cells was 36.3 ± 8.3. FITC-PNA, which is commercial PNA with a fluorescent probe, was substituted for the imaging agent. When the PNA concentration of FITC-PNA was adjusted to be equivalent to that of the imaging agent, the fluorescence intensity of the FITC-PNA-bound T47D cells was 2.48 ± 4.2, which was less than one-tenth of the fluorescence intensity of the imaging agent-bound T47D cells. It is considered that there is no significant difference between the affinities of the imaging agent and FITC-PNA for Gal-β(1-3)GalNAc. Data have demonstrated that the fluorescence intensity of the imaging agents was much higher than that of FITC-PNA at an equivalent amount of PNA. The difference in the fluorescence intensities may relate to the fluorescent quantum

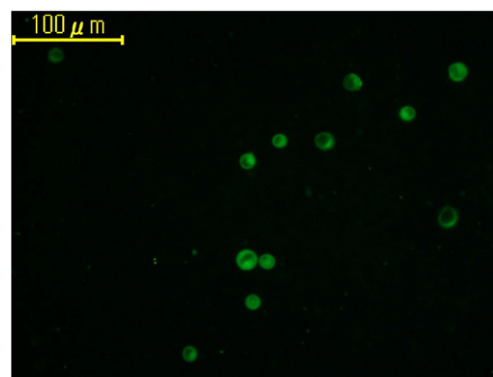


**Fig. 2.** Fluorescence microphotograph of the T47D cells incubated with PNA-immobilized fluorescent nanospheres with surface PNVA chains encapsulating coumarin 6 (imaging agents) in PBS with calcium and magnesium ions at 37 °C for 30 min. The picture was obtained using the fluorescence microscope (magnification: ×400; excitation: 470–495 nm; emission: 510–550 nm; exposure: 1/60 of a second).

Table 4  
Fluorescence intensity of various human cells after incubation with imaging agents (mean±s.d., n>5)

| Cultured human cells                   |         | Fluorescence intensity |
|--|---------|------------------------|
| Breast ductal carcinoma cell line      | T47D    | 36.3±8.3 <sup>a</sup>  |
| Colorectal adenocarcinoma cell line    | HT-29   | 30.4±4.1 <sup>a</sup>  |
|  | HCT-116 | 22.4±6.9 <sup>a</sup>  |
|  | LS174T  | 20.4±7.6 <sup>a</sup>  |
|  | HCT-15  | 16.2±6.4 <sup>a</sup>  |
|  | Caco-2  | 15.1±4.2 <sup>a</sup>  |
|  | SW480   | 10.1±4.6               |
| Epithelial cell of the small intestine |         | 8.72±0.56              |

<sup>a</sup> Statistically significant difference from data of normal epithelial cells.

efficiency of coumarin 6 encapsulated into the nanospheres and/or the amount of the dye per gram of PNA.

We next examined the biorecognition of the imaging agent against several types of human colorectal cancer cells. The expression of the TF antigen in HT-29, LS174T, Caco-2, and SW480 has been reported in the literature [19–20,45,46]; however, it appeared that the expression of the TF antigen in HCT-116 and HCT-15 has not been confirmed. Cultured human small intestinal epithelial cells were used as a negative control. It is predicted that Gal-β(1-3)GalNAc is masked by oligosaccharide side chain extension or sialylation in these normal cells. As shown in Table 4, the fluorescence intensity of the cancer cells derived from the imaging agent was higher than that of the normal epithelial cells. The difference between cancer cells and normal cells with regard to biorecognition probably resulted from the presence or absence of the surface carbohydrate residues. There were differences in the intensity of fluorescence among the cancer cells. A statistically significant increase in the fluorescence intensity of the cancer cells other than SW480 was observed in comparison with that of the normal epithelial cells. The order of the fluorescence intensity possibly corresponded to the expression level of the TF antigen. The quantification of the expression level was examined using immunofluorometric cell staining; however, the validity of this method has not been established due to its insufficient sensitivity (data not shown).

### 3.4. Targeting of the imaging agent against the orthotopic human colorectal tumor *in vivo*

We evaluated the *in vivo* performance of the imaging agent by using a human colorectal cancer orthotopic animal model. In this study, animals bearing tumors on the large intestinal mucosa are required because the imaging agent has been designed to recognize the tumor-derived changes on the mucosal side of cells. Two types of orthotopic models have been reported: the implantation of cultured human colorectal cancer cells in the large intestine of immune-deficient animals such as nude mice [47], and the implantation of tumor tissues in the intestine [37–40]. In the latter model, which has been developed by Hoffman et al., cultured cancer cells are first xenografted onto the flank of nude mice, and matured tumor tissues are next transplanted in the large intestine of other animals by surgical orthotopic implantation. In both models, cancer cells and tumor tissues are implanted on the serosa of the large intestine. Therefore, we examined the period that is required for the mucosal invasion of tumor tissues implanted on the large intestinal serosa by using the latter model. Histological examination showed that tumor tissues invaded the mucosal side of the epithelial cells when mice were maintained for at least 2 weeks after implantation (data not shown).

Coumarin 6, which was encapsulated into the nanosphere core, exhibits a fluorescence emission spectra at 510–550 nm. It is known that the autofluorescence in the body is seen in spectra similar to

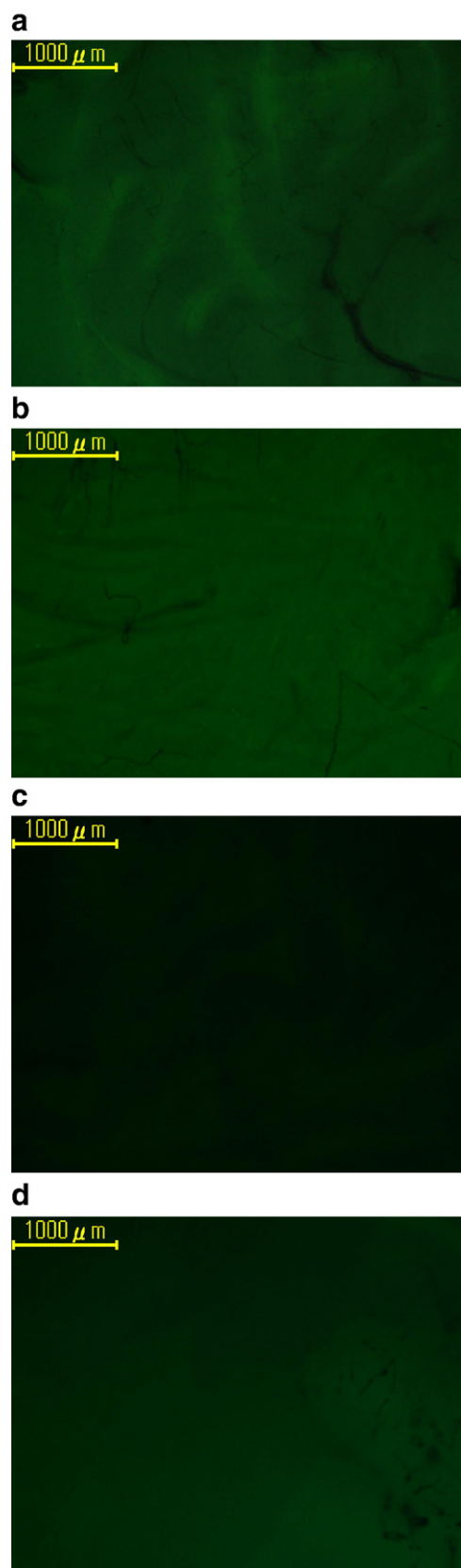
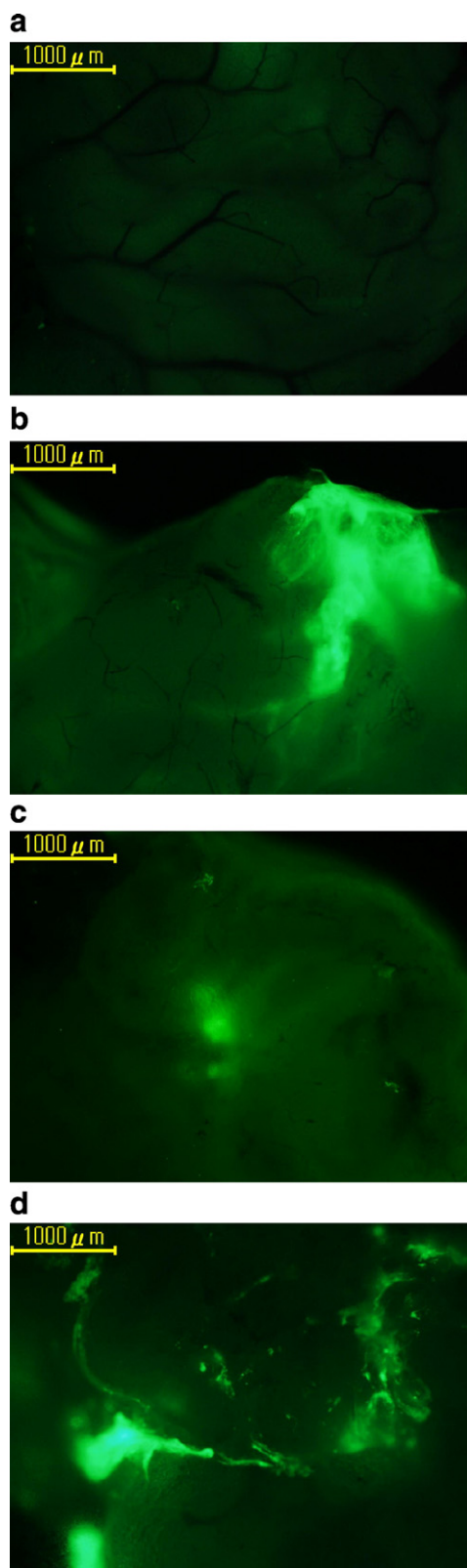


Fig. 3. Fluorescence microphotographs of the large intestinal mucosa in normal nude mice (a, c) and HT-29-RFP tumor tissues-implanted nude mice (b, d). Pictures were obtained using the fluorescence microscope (magnification: ×40; excitation: 470–495 nm; emission: 510–550 nm). Autofluorescence of the mucosa was observed at an exposure time of 1/15 of a second (a, b) and 1/30 of a second (c, d).



**Fig. 4.** Fluorescence microphotographs of the large intestinal mucosa in normal nude mice (a) and HT-29-RFP tumor tissues-implanted nude mice (b–d). Mice were sacrificed and a ca. 3-cm loop of the ascending colon was prepared. The luminal side of the colon was contacted with imaging agents for 30 min, washed with calcium ions-containing PBS, and then observed under the fluorescence microscope (magnification:  $\times 40$ ; excitation: 470–495 nm; emission: 510–550 nm; exposure: 1/60 of a second). Pictures b, c, and d correspond to fluorescence microphotographs of the mucosa in tumor tissues-implanted nude mice sacrificed at 22nd, 39th, and 48th day, respectively, after the surgical orthotopic implantation. In these three cases, the loop of the colon bearing tumor tissues was prepared.

those of coumarin 6 [13,14]. Thus, the large intestinal mucosa in normal and HT-29-RFP tumor tissue-implanted nude mice was first observed under fluorescence microscopy in the absence of imaging agents. As shown in Fig. 3, weak autofluorescence was observed on the mucosal surface, irrespective of the tumor implantation when the mucosa was observed at an exposure time of 1/15 of a second. However, the autofluorescence almost disappeared in both mice when the exposure time was halved. Nonspecific interactions between normal tissues and imaging agents were subsequently examined. Weak fluorescence was extensively observed on the mucosal surface when the exposure time was set as 1/30 of a second, which was free from autofluorescence (data not shown). It appeared that the fluorescence observed was derived from imaging agents bound to normal tissues nonspecifically. However, as shown in Fig. 4a, the fluorescence intensity was extremely low when the mucosal surface was observed under fluorescence microscopy at an exposure time of 1/60 of a second. This indicated that the nonspecific interactions between normal tissues and imaging agents were not so strong. The same test was performed for HT-29-RFP tumor tissue-implanted nude mice. The exposure time was set as 1/60 of a second during which nonspecific interactions between normal tissues and imaging agents were barely observed. As shown in Fig. 4b, c, and d, the strong fluorescence was observed at several sites of the large intestinal mucosa in tumor tissue-implanted mice treated with the imaging agent. The mucosal invasion in the tissues was confirmed by histological evaluation after performing biorecognition (data not shown). Specific accumulation of the imaging agent was not observed when nude mice that did not undergo tumor implantation were used (Fig. 4a). The accumulation of the imaging agents on the large intestinal mucosa in the orthotopic human colorectal cancer model indicated that the imaging agents bound to HT-29-RFP-derived tumor tissues with high affinity and specificity.

It seems that PNA-immobilized fluorescent nanospheres with surface PNVA chains encapsulating coumarin 6 are a potential candidate for use as a colonoscopic imaging agent. It is anticipated that small-sized early colorectal cancer is detected by observing a clear fluorescence contrast between the normal and tumor tissues using a fluorescence endoscope. However, several issues should be clarified. The macroscopic evaluation for the imaging ability was completed successfully, as shown in this report; however, the microscopic evaluation has not yet been performed. The excision of the mucosa under the microscope will prove that the bright and dark areas correspond to the presence and absence of mucosal invasion, respectively. Figs. 3 and 4 show that coumarin 6-based imaging overcame the autofluorescence of the mucosa. However, the replacement of coumarin 6 with near-infrared fluorescence imaging dyes may be effective for enhancing the accuracy of the diagnosis. We also hope that our system is evaluated clinically in the future. Re-design of imaging agents may be required from the standpoints of clinical use. For instance, a non-biodegradable covalent bond is another option to immobilize the dye into nanosphere cores because it assures for a hundred-percent non-release of the dye from nanospheres in a rigorous environment [48,49], although the strong hydrophobic interaction between coumarin 6 and polystyrene cores was observed. The productivity, specifications, and the chemical stability of imaging agents should be also examined. Further experiments will be discussed in future reports.

#### 4. Conclusions

PNA-immobilized fluorescent nanospheres with surface PNVA chains encapsulating coumarin 6 were designed as an endoscopic imaging agent for the detection of early colorectal cancer. Coumarin 6 was encapsulated efficiently into the polystyrene cores of nanospheres during the formation of their core-corona type structure. In vitro studies on the interactions between imaging agents and various types of cultured human cells demonstrated that the imaging agent

bound to the TF antigen-expressing cancer cells with high affinity and specificity; this was due to the recognition by the imaging agent of Gal- $\beta$ (1–3)GalNAc, the terminal sugar of the antigen. In vivo studies further indicated that the imaging agent bound to HT-29-RFP-derived tumor implanted orthotopically in the large intestine of nude mice with high affinity and specificity. It seemed that these fluorescent nanospheres are suitable as an imaging agent for fluorescence colonoscopy.

## Acknowledgments

This work was financially supported in part by a grant-in-aid for scientific research (No. 18590160) from the Ministry of Education, Culture, Sports, Sciences and Technology of Japan (MEXT) and a grant-in-aid from the Sagawa foundation for promotion of cancer research. The authors thank Showa Denko Co., Takara Bio Inc. (Otsu, Japan), and Applied Medical Research Inc. (Osaka, Japan) for the gift of NVA monomers, for the experiments and data analysis of immunofluorometric cell staining, and for the histological evaluation of tumor tissues, respectively.

## References

- [1] A. Jemal, R. Siegel, E. Ward, T. Murray, J. Xu, C. Smigal, M.J. Thun, Cancer statistics, *CA Cancer J. Clin.* 56 (2) (2006) 106–130.
- [2] <http://www.cancer.gov>.
- [3] G.C. Balch, A. De Meo, J.G. Guillem, Modern management of rectal cancer: a 2006 update, *World J. Gastroenterol.* 12 (20) (2006) 3186–3195.
- [4] T. Muto, M. Oya, Recent advances in diagnosis and treatment of colorectal T1 carcinoma, *Dis. Colon Rectum* 46 (10 Suppl.) (2003) S89–S93.
- [5] W.V. Harford, Colorectal cancer screening and surveillance, *Surg. Oncol. Clin. N. Am.* 15 (1) (2006) 1–20.
- [6] D. Lieberman, Screening for colorectal cancer in average-risk populations, *Am. J. Med.* 119 (9) (2006) 728–735.
- [7] T. Ponchon, Endoscopic mucosal resection, *J. Clin. Gastroenterol.* 32 (1) (2001) 6–10.
- [8] S. Kudo, Y. Tamegai, H. Yamano, Y. Imai, E. Kogure, H. Kashida, Endoscopic mucosal resection of the colon: the Japanese technique, *Gastrointest. Endosc. Clin. N. Am.* 11 (3) (2001) 519–535.
- [9] B. Rembacken, T. Fujii, H. Kondo, The recognition and endoscopic treatment of early gastric and colonic cancer, *Best Prac. Res. Clin. Gastroenterol.* 15 (2) (2001) 317–336.
- [10] H. Kashida, S. Kudo, Early colorectal cancer: concept, diagnosis, and management, *Int. J. Clin. Oncol.* 11 (1) (2006) 1–8.
- [11] J.J. Tischendorf, H.E. Wasmuth, A. Koch, H. Hecker, C. Trautwein, R. Winograd, Value of magnifying chromoendoscopy and narrow band imaging (NBI) in classifying colorectal polyps: a prospective controlled study, *Endoscopy* 39 (12) (2007) 1092–1096.
- [12] R.S. DaCosta, B.C. Wilson, N.E. Marcon, Fluorescence and spectral imaging, *Sci. World J.* 7 (2007) 2046–2071.
- [13] S. Anandasabapathy, Endoscopic imaging: emerging optical techniques for the detection of colorectal neoplasia, *Curr. Opin. Gastroenterol.* 24 (1) (2008) 64–69.
- [14] F.J. van der Broek, P. Fockens, E. Dekker, New development in colonic imaging, *Aliment Pharmacol Ther.* (Suppl. 2) (2007) 91–99.
- [15] M. Hirata, S. Tanaka, S. Oka, I. Kaneko, S. Yoshida, M. Yoshihara, K. Chayama, Evaluation of microvessels in colorectal tumors by narrow band imaging magnification, *Gastrointest. Endosc.* 66 (5) (2007) 945–952.
- [16] K. Kelly, H. Alencar, M. Funovics, U. Mahmood, R. Weissleder, Detection of invasive colon cancer using a novel, targeted, library-derived fluorescent peptide, *Cancer Res.* 64 (17) (2004) 6247–6251.
- [17] K. Hiwatari, S. Sakuma, K. Iwata, Y. Masaoka, M. Kataoka, H. Tachikawa, Y. Shoji, S. Yamashita, Poly(N-vinylacetamide) chains enhance lectin-induced biorecognition through the reduction of nonspecific interactions with non-targets, *Eur. J. Pharm. Biopharm.* 70 (2) (2008) 453–461.
- [18] C.R. Boland, J.A. Roberts, Quantitation of lectin binding sites in human colon mucins by use of peanut and wheat germ agglutinin, *J. Histochem. Cytochem.* 36 (10) (1988) 1305–1307.
- [19] B.J. Campbell, I.A. Finnie, E.F. Hounsell, J.M. Rhodes, Direct demonstration of increased expression of Thomsen–Friedenreich (TF) antigen from colonic adenocarcinoma and ulcerative colitis mucin and its concealment in normal mucin, *J. Clin. Invest.* 95 (2) (1995) 571–576.
- [20] R. Singh, B.J. Campbell, L.-G. Yu, D.G. Fernig, J.D. Milton, R.A. Goodlad, A.J. FitzGerald, J.M. Rhodes, Cell surface-expressed Thomsen–Friedenreich antigen in colon cancer is predominantly carried on high molecular weight splice variants of CD44, *Glycobiology* 11 (7) (2001) 587–592.
- [21] E. Dabelsteen, Cell surface carbohydrates as prognostic markers in human carcinomas, *J. Pathol.* 179 (4) (1996) 358–369.
- [22] M.A. Clark, B.H. Hirst, M.A. Jepson, Lectin-mediated mucosal delivery of drugs and microparticles, *Adv. Drug Deliv. Rev.* 43 (2–3) (2000) 207–223.
- [23] C. Bies, C.-M. Lehr, J.F. Woodley, Lectin-mediated drug targeting: history and applications, *Adv. Drug Deliv. Rev.* 56 (4) (2004) 425–435.
- [24] F. Gabor, E. Bogner, A. Weissenboeck, M. Wirth, The lectin-cell interaction and its implications to intestinal lectin-mediated drug delivery, *Adv. Drug Deliv. Rev.* 56 (4) (2004) 459–480.
- [25] J.M. Rini, Lectin structure, *Annu. Rev. Biophys. Biomol. Struct.* 24 (1995) 551–577.
- [26] S. Wróblewski, P. Kopečková, B. Řihová, J. Kopeček, Lectin-HPMA copolymer conjugates: potential oral drug carriers for targeting diseased tissues, *Macromol. Chem. Phys.* 199 (11) (1998) 2601–2608.
- [27] S. Wróblewski, M. Berenson, P. Kopečková, J. Kopeček, Biorecognition of HPMA copolymer–lectin conjugates as an indicator of differentiation of cell-surface glycoproteins in development, maturation, and diseases of human and rodent gastrointestinal tissues, *J. Biomed. Mater. Res.* 51 (3) (2000) 329–342.
- [28] S. Wróblewski, M. Berenson, P. Kopečková, J. Kopeček, Potential of lectin-N-(2-hydroxypropyl)methacrylamide copolymer–drug conjugates for the treatment of pre-cancerous conditions, *J. Control. Release* 74 (1–3) (2001) 283–293.
- [29] S. Sakuma, Z.-R. Lu, P. Kopečková, J. Kopeček, Biorecognizable HPMA copolymer–drug conjugates for colon-specific delivery of 9-aminocamptothecin, *J. Control. Release* 75 (3) (2001) 365–379.
- [30] S. Sakuma, M. Hayashi, M. Akashi, Design of nanoparticles composed of graft copolymers for oral peptide delivery, *Adv. Drug Deliv. Rev.* 47 (1) (2001) 21–37.
- [31] S. Sakuma, R. Sudo, N. Suzuki, H. Kikuchi, M. Akashi, M. Hayashi, Mucoadhesion of polystyrene nanoparticles having surface hydrophilic polymeric chains in the gastrointestinal tract, *Int. J. Pharm.* 177 (2) (1999) 161–172.
- [32] S. Sakuma, R. Sudo, N. Suzuki, H. Kikuchi, M. Akashi, Y. Ishida, M. Hayashi, Behavior of mucoadhesive nanoparticles having hydrophilic polymeric chains in the intestine, *J. Control. Release* 81 (3) (2002) 281–290.
- [33] S. Sakuma, N. Suzuki, R. Sudo, K. Hiwatari, A. Kishida, M. Akashi, Optimized chemical structure of nanoparticles as carriers for oral delivery of salmon calcitonin, *Int. J. Pharm.* 239 (1–2) (2002) 185–195.
- [34] M. Akashi, T. Niikawa, T. Serizawa, T. Hayakawa, M. Baba, Capture of HIV-1 gp120 and virions by lectin-immobilized polystyrene nanospheres, *Bioconjug. Chem.* 9 (1) (1998) 50–53.
- [35] M. Akashi, M. Wada, S. Yanase, N. Miyauchi, Polymer drugs and polymeric drugs, II. Synthesis of water dispersible microspheres having 5-fluorouracil and theophylline using a water soluble macromonomer, *J. Polym. Sci. Part C: Polym. Lett.* 27 (1989) 377–380.
- [36] M.-Q. Chen, T. Serizawa, M. Li, C. Wu, M. Akashi, Thermosensitive behavior of poly(N-isopropylacrylamide) grafted polystyrene nanoparticles, *Polym. J.* 35 (12) (2003) 901–910.
- [37] S. Togo, H. Shimada, T. Kubota, A. Moossa, R.M. Hoffman, Host organ specifically determines cancer progression, *Cancer Res.* 55 (3) (1995) 681–684.
- [38] M. Yang, L. Li, P. Jiang, A.R. Moossa, S. Penman, R.M. Hoffman, Dual-color fluorescence imaging distinguishes tumor cells from induced host angiogenic vessels and stromal cells, *Proc. Natl. Acad. Sci. USA* 100 (24) (2003) 14259–14262.
- [39] Y. Amoh, M. Yang, L. Li, J. Reynoso, M. Bouvet, A.R. Moossa, K. Katsunaka, R.M. Hoffman, Nestin-linked green fluorescent protein transgenic nude mouse for imaging human tumor angiogenesis, *Cancer Res.* 65 (12) (2005) 5352–5357.
- [40] <http://www.anticancer.com/>.
- [41] N. Sharon, H. Lis, Lectins as cell recognition molecules, *Science* 246 (4927) (1989) 227–234.
- [42] A.P. Corfield, B.F. Warren, Mucus glycoproteins and their role in colorectal disease, *J. Pathol.* 180 (1) (1996) 8–17.
- [43] F. Gabor, M. Stangl, M. Wirth, Lectin-mediated bioadhesion: binding characteristics of plant lectins on the erythrocyte-like cell lines Caco-2, HT-29 and HCT-8, *J. Control. Release* 55 (2–3) (1998) 131–142.
- [44] F. Hanisch, T. Stadie, F. Deutzmann, J. Peter-Katalinic, MUC1 glycoforms in breast cancer-cell line T47D as a model for carcinoma-associated alterations of O-glycosylation, *Eur. J. Biochem.* 236 (1) (1996) 318–327.
- [45] J. Samuel, A. Noujaim, G. MacLean, M. Suresh, B. Longenecker, Analysis of human tumor associated Thomsen–Friedenreich antigen, *Cancer Res.* 50 (15) (1990) 4801–4808.
- [46] F. Schneider, W. Kemmer, W. Haensch, G. Franke, S. Gretschel, U. Karsten, P. Schlag, Overexpression of sialyltransferase CMP-sialic acid: Gal $\beta$ 1,3GalNAc-R  $\alpha$ 6-sialyltransferase is related to poor patient survival in human colorectal carcinoma, *Cancer Res.* 61 (11) (2001) 4605–4611.
- [47] M. Zamai, M. vandeVen, M. Farao, E. Gratton, A. Ghiglieri, M. Castelli, E. Fontana, R. d'Argy, A. Fiorino, E. Pesenti, A. Suarato, V. Caiola, Camptothecin poly[N-(2-hydroxypropyl)methacrylamide] copolymers in antitopoisomerase–I tumor therapy: intratumor release and antitumor efficacy, *Mol. Cancer Ther.* 2 (1) (2003) 29–40.
- [48] T. Akagi, M. Higashi, T. Kaneko, T. Kida, M. Akashi, Hydrolytic and enzymatic degradation of nanoparticles based on amphiphilic poly( $\gamma$ -glutamic acid)-graft-l-phenylalanine copolymers, *Biomacromolecules* 7 (2006) 297–303.
- [49] S. Sakuma, T. Sagawa, Y. Masaoka, M. Kataoka, S. Yamashita, Y. Shirasaka, I. Tamai, Y. Ikumi, T. Kida, M. Akashi, Stabilization of enzyme-susceptible glucoside bonds of phloridzin through conjugation with poly( $\gamma$ -glutamic acid). *J. Control. Release*, in press.